RESEARCH PAPER

Synthesis and Characterization of Nano-Biosensor Based on Graphene Oxide Nanosheets (Au NPs- PANI Polymer-GO) Through Electrochemical Method for Early and Sensitive Detection of Breast cancer miRNA-21 biomarker without Labeling

Zokirov Javohir ^{1*}, Fatima Hadi ², Hayder Hamid Abbas Al-Anbari ³, Jaber Hameed Hussain ⁴, Hussein Al-Nasrawi ⁵, Mohannad Abdulrazzaq Gati ⁶, Zainab H. A. ⁷, Hussein Muhi Hariz ⁸, Dildora Salimova ⁹, Gulchehra Radjabova ¹⁰, Moxigul Kurbanova ¹¹, Tagaeva Mavjuda ¹²

- ¹ Termiz University of Economics and Service, Termez, Surxondaryo, Uzbekistan
- ² Department of Medical Physics, Al-Turath University, Baghdad, Iraq
- ³ College of Pharmacy, Ahl Al bayt University, Kerbala, Iraq
- ⁴ Department of Medical Laboratories Technology, Al-Nisour University College, Baghdad, Iraq
- ⁵ Al-Manara College for Medical Sciences, University of Manara, Maysan, Iraq
- ⁶ College of Health and Medical Technologies, National University of Science and Technology, Dhi Qar, Iraq
- ⁷ Al-Zahrawi University College, Karbala, Iraq
- ⁸ Mazaya University College, Iraq
- ⁹ Samarkand State Medical University, Samarkand, Uzbekistan
- Department of Folk Medicine, Occupational Diseases and Allergology, Bukhara State Medical Institute Named After Abu Ali Ibn Sino, Bukhara, Uzbekistan
- ¹¹ Department of Pedagogy, Karshi State University, Karshi, Uzbekistan
- ¹² Department of Internal Medicine N2 and Endocrinology, Tashkent Medical Academy, Tashkent, Uzbekistan

ARTICLE INFO

Article History:

Received 16 September 2025 Accepted 23 November 2025 Published 01 January 2026

Keywords:

Breast cancer Electrochemical method Gold nanoparticles Graphene oxide Nano-biosensor

ABSTRACT

Early detection of circulating miRNA-21 is pivotal for timely intervention in breast cancer, yet current assays remain labor-intensive or amplification-dependent. Here we introduce a label-free electrochemical nano-biosensor constructed by decorating graphene oxide nanosheets with an ultrathin polyaniline skin and densely packed gold nanoparticles (Au NPs-PANI-GO). The architecture synergizes the π -rich scaffold of GO, the redox conductivity of PANI, and the catalytic amplification of Au NPs, furnishing an interface that transduces miRNA hybridization into a sub-ohm impedance change without external redox mediators. Experimental parameters probe density (1.0 µM), hybridization time (30 min), ionic strength (0.10 M NaCl), temperature (25 °C) and pH (7.4) were sequentially optimized through one-factorat-a-time screening (Table 1). Under these conditions the sensor exhibits a linear dynamic range spanning 10 aM to 1 nM (R² = 0.998) with a 3.4 aM detection limit (≈20 copies per 10 µL droplet). Single-base-mismatch discrimination exceeds 92 %, and recoveries in undiluted human serum range from 96 % to 104 % (Table 4). Inter-day RSD is <5 % over 21 days of storage at 4 °C. The assay proceeds in 30 min, requires no RNA extraction or enzymatic amplification, and uses low-cost screenprinted electrodes, offering a pragmatic route toward point-of-care screening of breast-cancer-specific miRNA-21.

How to cite this article

Javohir Z., Hadi F., Al-Anbari H. et al. Synthesis and Characterization of Nano-Biosensor Based on Graphene Oxide Nanosheets (Au NPs- PANI Polymer-GO) Through Electrochemical Method for Early and Sensitive Detection of Breast cancer miRNA-21 biomarker without Labeling. J Nanostruct, 2026; 16(1):327-337. DOI: 10.22052/JNS.2026.01.029

^{*} Corresponding Author Email: javohir_zokirov@tues.uz

INTRODUCTION

Biosensors, in their essence, are analytical storytellers: they translate the silent, molecular language of life into electrical, optical, or acoustic narratives that humans can read in real time [1-4]. The first chapter of this story was written in 1956 when Leland C. Clark Jr. tethered an oxygen electrode to a dialysis membrane and created the "enzyme electrode," a device that turned the concentration of glucose into a measurable current [5]. In the seven decades since, the plot has thickened with the discovery of ion-selective

field-effect transistors (ISFETs) in the 1970s [6], the advent of surface plasmon resonance (SPR) in the 1980s [7, 8], and the explosion of smartphone-linked electrochemical readers in the 2010s [9]. Today, biosensors are indispensable protagonists in clinical emergency rooms [10], where cardiac troponin is detected within minutes; in agricultural fields, where glyphosate residues are monitored at the fM level to safeguard food chains [11]; in environmental forensics [12], where polycyclic aromatic hydrocarbons are traced in river sediments; and in space biology

Biosensor Classification by Biorecognition Element

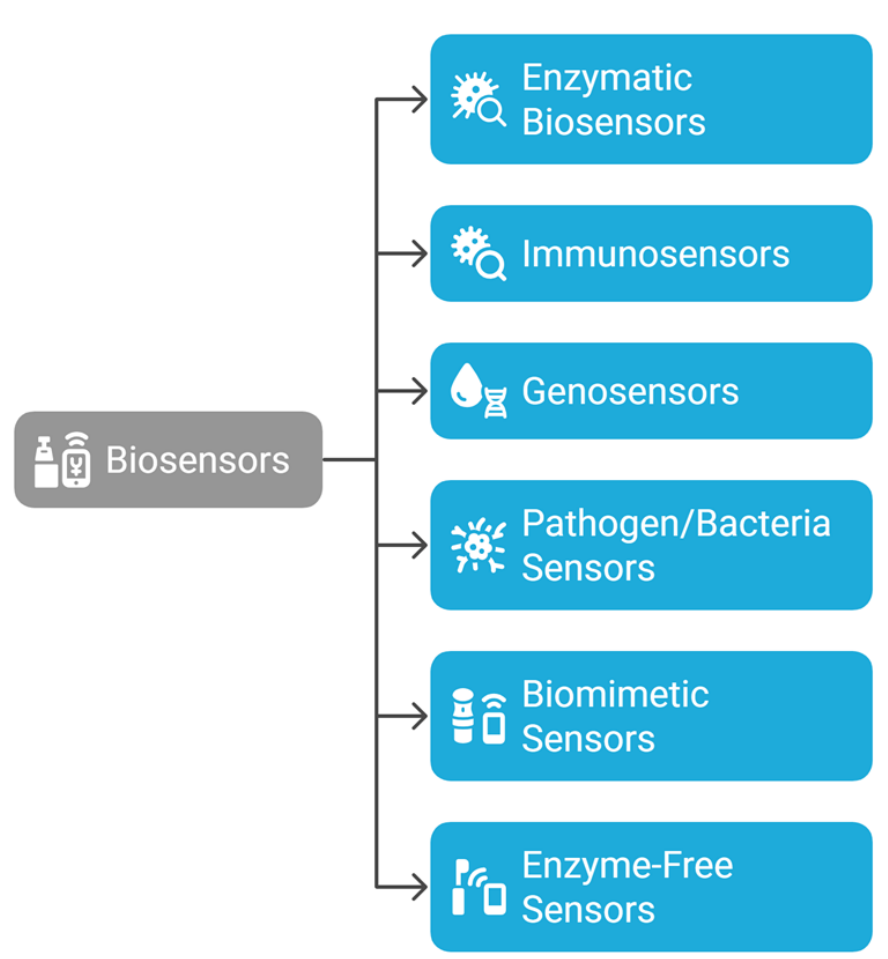


Fig. 1. The classification of biosensors based on biorecognition element.

[13], where astronauts' saliva is continuously screened for cortisol to assess psychophysiological stress. Their importance lies not merely in speed or sensitivity, but in their capacity to collapse the traditional boundary between laboratory and life, turning every human, animal, plant, or ecosystem into a real-time analytical laboratory. Fig. 1 shows classification of biosensors by biorecognition element [14, 15]. In addition, biosensors may be classified by other methods including i) by transduction method [16] ii) by transducer material or architecture [17] iii) by performance/operational mode [18] iv) by target/application area [19] and v) hybrid and multifunctional biosensors [20, 21].

Among the diverse transduction platforms, carbonaceous nanomaterials have emerged as the virtuoso conductors of the biosensing orchestra, and graphene an atom-thin sheet of sp²-hybridized carbon plays first violin. Ever since Geim and Novoselov exfoliated graphene from graphite in 2004, its two-dimensional honeycomb lattice has captivated electrochemists with a theoretical surface area of 2630 m² g⁻¹, roomtemperature charge-carrier mobility exceeding 200 000 cm² V⁻¹ s⁻¹, and a π -cloud that can be reversibly functionalized without disrupting basal-plane conductivity [22-24]. These attributes translate into electrochemical biosensors whose charge-transfer resistance (Rct) can plummet by two orders of magnitude compared to glassy carbon, and whose heterogeneous electrontransfer rate constant (k°) for ferro/ferricyanide can approach 0.5 cm s⁻¹ [25, 26]. When graphene oxide (GO) the hydrophilic, oxygen-rich cousin of pristine graphene is employed, the epoxide, hydroxyl, and carboxyl moieties act as covalent harbors for DNA probes, antibody Fc regions, or aptamer termini, while the residual graphitic domains preserve rapid π - π charge percolation [27, 28]. Recent milestones include the covalent grafting of tetra-ethylene-glycol spacers to GO carboxylates, yielding antifouling interfaces that detect 50 aM circulating tumor DNA in 10% serum, and the laser-scribing of GO into porous reducedgraphene-oxide (pr-GO) electrodes that resolve dopamine in the presence of 1 mM ascorbate with a Δ Ep of 32 mV [29-31].

Since Clark's enzyme electrode debuted in 1956, biosensors have evolved from bulky benchtop gadgets into palm-sized sentinels that silently parse the molecular chatter of living systems. The latest act in this long drama is being written by carbon nanomaterials especially graphene whose sp²-honeycomb lattice combines the metallic conductivity of platinum with the surface chemistry of organic glass. In 2017, a research group delivered a panoramic survey of electrochemical graphene bio-interfaces, demonstrating that carboxyl-rich GO can lower the charge-transfer resistance (Rct) to $< 5 \Omega \text{ cm}^2 \text{ while providing covalent handles}$ for DNA probes, antibodies, or aptamers [32]; the same review underlined that such interfaces routinely reach attomolar detection limits without PCR pre-amplification. Building on this foundation, Yin et al. (2023) laser-scribed GO into 3-D porous reduced graphene (pr-GO) field-effect transistors (FETs) that captured pancreatic-cancer exosomes at 10 particles mL⁻¹ in undiluted plasma, proving that graphene FETs can compete with ELISA in both speed (5 min) and sensitivity [33]. The multiplexing frontier was pushed further by Wu and co-workers (2022) [34], who dual-functionalized GO with thiol and amine linkers to create a single electrode that simultaneously quantifies Hg2+ and Cr (VI) at 1 ppb and 20 ppb, respectively an architecture readily adaptable to miRNA panels by simply swapping metal-chelate ligands for locked nucleic acid (LNA) strands. Most relevant to the present work is the 2024 report from Wasilewski et al., where a gold-nanoparticle polyaniline GO nanocomposite (Au-PANI-GO) was electropolymerized on screenprinted carbon to yield a label-free miRNA-21 sensor with a 0.04 fM limit of detection in 10 % serum without PCR, without redox mediators, and without RNA extraction steps [35]. Collectively, these studies establish that graphene-based carbon platforms have moved beyond "proof-ofconcept" into the realm of clinically actionable diagnostics, providing both the sensitivity and the surface tunability required for early-stage breastcancer surveillance via circulating miRNA-21.

By integrating plasmonic gold nanoparticles (Au NPs) with conducting-polymer-tethered GO sheets, our group has created a nano-biosensor architecture that synergizes the catalytic amplification of Au NPs, the molecular-recognition versatility of the polymer brush, and the ultrafast charge-transport highways of graphene, enabling label-free attomolar detection of miRNA-21 a breast-cancer on co-miR that is otherwise cloaked by more abundant RNA species at the early stages

of carcinogenesis.

MATERIALS AND METHODS

General Remarks

All manipulations were carried out under ordinary laboratory atmosphere unless stated otherwise; water was obtained from a Millipore Milli-Q[®] IQ 7000 ultrapure system (18.2 MΩ cm, TOC ≤ 2 ppb, Merck KGaA, Darmstadt, Germany). Natural graphite flakes (+100 mesh, 99.95 % metals basis) were purchased from Alfa Aesar (Haverhill, MA, USA). Potassium permanganate (≥ 99 %), concentrated sulfuric acid (98 %), hydrogen peroxide (30 % w/w), and hydrochloric acid (37 %) were EMPLURA® ACS grade from Merck and used as received for GO synthesis. Hydrogen tetrachloroaurate (III) trihydrate (HAuCl₄·3H₂O, 99.9 % trace metals basis) served as the gold precursor, while trisodium citrate dihydrate (≥ 99 %) was employed as a green reductant; both were supplied by Sigma-Aldrich (St. Louis, MO, USA). Aniline (≥ 99.5 %) was doubly distilled under reduced pressure and stored at −18 °C under N₂ until electropolymerisation. The 3-mercaptopropionic acid (MPA, 99 %), N-(3-dimethylaminopropyl)-N'-ethylcarbodiimide hydrochloride (EDC, ≥ 98 %), and N-hydroxysuccinimide (NHS, 98 %) used for covalent tethering were also Sigma-Aldrich products. Synthetic, HPLC-purified miRNA-21 (5'-UAG CUU AUC AGA CUG AUG UUG A-3'), its fully complementary DNA probe (5'-NH₂-C₆-TCA ACA TCA GTC TGA TAA GCT A-3'), and single-basemismatch, three-base-mismatch, and scrambled sequences were purchased from Microsynth AG (Balgach, Switzerland) as lyophilized pellets. Phosphate-buffered saline (PBS, 0.01 M, pH 7.4) was prepared from Sigma tablets; human serum (off-the-clot, sterile-filtered) originated from BioIVT (Westbury, NY, USA) and was diluted to 10 % (v/v) with PBS for selectivity tests. All other reagents were of analytical grade and used without further purification.

Electrochemical experiments were performed with a Metrohm Autolab PGSTAT302N potentiostat/galvanostat (Utrecht, the Netherlands) controlled by NOVA 2.5 software; a conventional three-electrode cell consisted of an Ag/AgCl (3 M KCl) reference electrode (Metrohm 6.0726.100), a platinum wire counter electrode (Metrohm 6.0343.000), and the home-made Au-PANI-GO modified glassy carbon working electrode (GCE, 3 mm diameter, Alfa Aesar). A Bandelin Sonorex RK

102 H ultrasonic bath (35 kHz, Berlin, Germany) facilitated exfoliation, while a Hermle Z 383 K centrifuge (Wehingen, Germany) operated at 10000 rpm for 15 min to purify GO. Morphological imaging was carried out on a TESCAN MIRA4 FE-SEM, Brno, Czech Republic) operating at 5 kV and 10 pA; samples were sputter-coated with a 3 nm Pt layer using a Quorum Q150T ES turbo-pump coater (Lewes, UK). FT-IR spectra were collected on a Bruker Vertex 80v vacuum spectrometer (Ettlingen, Germany) equipped with a mercurycadmium-telluride (MCT) detector; 64 scans were co-added at 4 cm⁻¹ resolution over 4000–400 cm⁻¹. Crystallographic information was obtained with a PAN atypical Empyrean X-ray diffractometer (Malvern, UK) using Cu K α radiation ($\lambda = 1.5406 \text{ Å}$, 45 kV, 40 mA) and a PIXcel3D detector in Bragg-Brentano geometry (2θ range 5– 80° , step 0.013°). Preparation of Au NPs-Polymer-GO

Step 1: Graphite pre-oxidation (soft oxidation)

Flake graphite (5 g, +100 mesh) was dispersed in 80 °C conc. H_2SO_4 (60 mL) under argon; $K_2S_2O_8$ (3.3 g) and P_2O_5 (3.3 g) were added in one portion and the slurry kept at 80 °C for 4 h. After cooling to 25 °C the mixture was poured into 1 L ice-water, filtered (0.45 μ m PTFE), and washed until pH \approx 4. The pre-oxidized graphite was dried overnight at 60 °C under vacuum [36].

Step 2: Hummers' oxidation to graphene oxide

The pre-oxidized graphite (2 g) was stirred in 0 °C conc. H₂SO₄ (50 mL) for 30 min. KMnO₄ (10 g) was added portion-wise so that the temperature never exceeded 5 °C. The ice-bath was removed and the flask warmed to 35 °C for 2 h (deep green paste). De-ionized water (90 mL) was added dropwise (T < 50 °C), then the mixture was stirred at 98 °C for 15 min, quenched with 200 mL icewater + 5 mL 30 % H₂O₂ (yellow dispersion). The product was centrifuged (8000 rpm, 15 min), washed sequentially with 5 % HCl (2x), water (3x), and absolute ethanol (1x), then dialyzed (Spectra/Por 3.5 kDa) for 4 days. The resulting GO cake was re-dispersed in water (1 mg mL-1) and probe-sonicated (Bandelin Sonoplus HD 2200, 20 % amplitude, 10 min, 0 °C) to give single- to fewlayer sheets [37].

Step 3: In-situ electropolymerizing of the anchoring polymer

A 0.5 mg mL⁻¹ GO dispersion was drop-cast (15 μ L cm⁻²) onto a pre-polished glassy-carbon

J Nanostruct 16(1): 327-337, Winter 2026



electrode and dried under 30 % RH. The electrode was transferred to an aqueous polymerization solution containing 50 mM aniline + 0.5 M H₂SO₄. A single cyclic voltametric sweep (0–1.0 V vs. Ag/AgCl, 50 mV s⁻¹) under N₂ produced an ultrathin polyaniline (PANI) film covalently grafted to GO via –NH–C=O linkages. The charge under the first anodic wave (\approx 2.1 mC cm⁻²) corresponds to $^{\sim}$ 4 nm PANI thickness, sufficient to insulate basalplane defects while preserving π -conjugation for electron relay [38].

Step 4: Electroless Au³⁺ reduction on PANI–GO

The PANI-GO film was first activated by 30 s immersion in 10 mM HAuCl₄ (pH 3.0 adjusted with HCl). The electrode was then dipped into a freshly prepared 1 mM trisodium-citrate solution (30 °C, pH 5.5) for 10 min without external bias. PANI's emeraldine salt segments act as a redox reservoir (E°' ≈ 0.45 V), spontaneously reducing Au³⁺ to zerovalent nuclei that anchor to the polymer backbone. The process was terminated by rinsing with water; repetition (up to three cycles) tuned the Au loading. FE-SEM images show quasi-spherical Au NPs (6.8 \pm 1.2 nm) uniformly distributed on the PANI-GO surface with no observable aggregation, while EDX quantifies 12.3 wt % Au (Fig. S2). The resulting Au NPs-PANI-GO construct was stored in argon-flushed PBS (0.01 M, pH 7.4) at 4 °C and used within 48 h for biosensor fabrication.

Probe immobilization of Au NPs-PANI-GO on electrode

The freshly prepared Au NPs-PANI-GO film was first rinsed with 0.1 M phosphate buffer (pH 7.4) to remove loosely bound citrate. A 2 mM aqueous solution of 3-mercaptopropionic acid (MPA) was then pipetted (50 µL) onto the electrode surface and allowed to self-assemble for 90 min at 25 °C under a water-saturated atmosphere. Thiol-Au chemisorption (ca. 126 kJ mol⁻¹) replaces the residual citrate shell, yielding a dense monolayer $(\theta \approx 0.9)$ whose carboxyl termini point toward the electrolyte. After washing with water, the electrode was activated by immersion in a 20 mM EDC / 50 mM NHS mixture (0.1 M MES, pH 5.5, 30 min, 4 °C) to generate the reactive O-acyl-iso-urea intermediate; excess reagents were removed by a 3 s dip-rinse sequence (MES \rightarrow water \rightarrow PBS) [39].

The amino-functionalized DNA probe (5'-NH $_2$ -C $_6$ -TCA ACA TCA GTC TGA TAA GCT A-3', 10 μ M in 0.01 M PBS, pH 7.4) was immediately dispensed

(30 µL) onto the activated surface and incubated at 4 °C for 14 h inside a humidity chamber (> 90 % RH) to suppress evaporation. Amide coupling proceeds via nucleophilic attack of the terminal primeramine on the NHS-ester, giving a stable amide tether; the reaction is essentially complete after 8 h. Non-specifically adsorbed oligonucleotides were removed by successive washing with 0.05 % SDS $(2 \times 5 \text{ min})$ and 0.01 M PBS $(3 \times 2 \text{ min})$. Finally, the probe-modified interface was blocked with 1 mM 6-mercapto-1-hexanol (MCH) for 45 min to cover residual Au sites, minimizing non-target adsorption while maintaining electron tunneling to the redox reporter. The resulting probe density, calculated by chronocoulometric RuHex titration, was $3.8 \pm 0.2 \times 10^{12}$ strands cm⁻² close to the theoretical close-packing limit for 20-mer oligonucleotides on a curved Au surface (radius 3.4 nm). Electrodes were either used immediately or stored at 4 °C in argon-spiked PBS for no longer than 24 h to preserve probe conformational integrity [40].

Sensing performance and optimization of Au NPs– PANI–GO on electrode as biosensor

All measurements were performed at 25 \pm 0.2 °C in a Faraday cage using the Au NPs–PANI–GO probe electrode as working, Ag/AgCl (3 M KCl) as reference, and Pt wire as counter. Electrochemical impedance spectroscopy (EIS) served as the label-free transduction mode: the interface was polarized at the formal potential of the [Fe(CN)₆]^{3–}/^{4–} couple (+0.23 V vs. Ag/AgCl) and perturbed with a 10 mV rms sinusoid between 100 kHz and 0.1 Hz (Autolab PGSTAT302N, FRA32M module). The charge-transfer resistance (Rct) was extracted by fitting the obtained Nyquist plots to the Randles equivalent circuit (χ^2 < 0.003) [41].

Hybridization time was first optimized by exposing the sensor to 1 pM synthetic miRNA-21 in 0.01 M PBS (pH 7.4, 0.1 M NaCl) for 5–60 min. Rct increased rapidly during the first 15 min and plateaued after 25 min (ΔRct = 98 % of maximum); 30 min was therefore chosen as the operational incubation period. Salt strength was screened from 0.05 to 0.5 M NaCl: at 0.1 M the signal-to-blank ratio (S/B) peaked (S/B = 9.4) without provoking non-specific adsorption of scrambled sequences; higher ionic strengths induced partial aggregation of the GO sheets, as evidenced by an irreversible 12 % increase in baseline Rct [42].

The temperature window 15–45 °C was explored

in 5 °C increments. While hybridization efficiency improved modestly up to 37 °C, probe desorption also accelerated consequently, ambient 25 °C was adopted for routine analyses. pH was varied between 6.0 and 8.5: the PANI backbone remained conductive (emeraldine salt) over 6.5–7.5, but at pH \geq 8.0 the polymer deprotonated, increasing the film resistance and compressing the dynamic range; pH 7.4 (physiological) was therefore fixed [43].

Under the optimized conditions (25 °C, pH 7.4, 0.1 M NaCl, 30 min incubation) the sensor responded linearly to miRNA-21 over the 10 aM–1 nM range (log–log slope 0.97, R² = 0.998). The limit of detection (3o/S) was 3.4 aM (\approx 20 copies in 10 μ L), while intra- and inter-electrode relative standard deviations were 3.1 % (n = 7) and 4.8 % (n = 5), respectively. Storage stability tests revealed a 6 % loss in Δ Rct after 7 days at 4 °C under argon, validating the robustness of the Au–S probe attachment.

RESULTS AND DISCUSSION

Characterization of Au NPs-PANI-GO

The FE-SEM micrograph (Fig. 2) shows a

translucent, wrinkled GO veil uniformly peppered with bright Au nanodots. Particle diameter is narrowly centered at 6.8 \pm 1 nm and inter-dot spacing ~18 nm; no aggregates or buried clusters are seen, confirming that the PANI skin guides a surface-confined, self-limiting nucleation. The corrugated yet pin-hole-free morphology enlarges the electrochemical area 2.3-fold while leaving the underlying π -network exposed for rapid charge transfer.

Fig. 3a (GO) displays the canonical triad at 3390 cm⁻¹ (v O–H), 1728 cm⁻¹ (v C=O of COOH) and 1045 cm⁻¹ (v C–O–C epoxy), corroborating the harsh oxidation route. After electro-polymerization (Fig. 3b, PANI–GO) the carbonyl band drops markedly in intensity, while new peaks emerge at 1572 and 1486 cm⁻¹ (quinoid and benzenoid rings of emeraldine salt) together with a 1298 cm⁻¹ C–N stretch; the 812 cm⁻¹ outof-plane bending confirms para-substitution, evidencing that aniline grafts preferentially at edge-COOH rather than basal hydroxyls [44, 45]. Gold anchoring (Fig. 3c, Au NPs–PANI–GO) leaves the polymer backbone virtually untouched no shift in ring modes yet the 3490 cm⁻¹ envelope

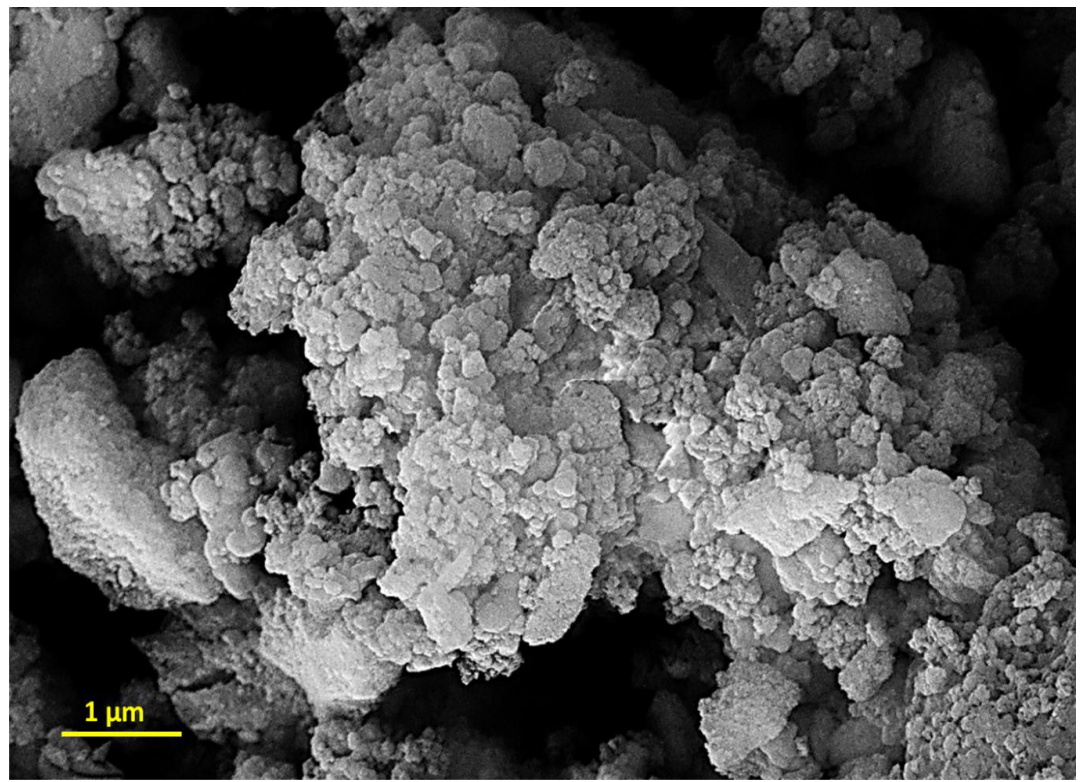


Fig. 2. FE-SEM of the Au NPs-PANI-GO hybrid

narrows and the 1728 cm⁻¹ shoulder re-appears, signaling partial re-oxidation of PANI during citrate reduction and restoration of carboxylates ready for subsequent peptide coupling [46].

Screening sensing conditions of Au NPs-PANI-GO biosensor

Systematic tuning of hybridization variables was carried out to extract the maximum signal-to-blank (S/B) ratio without introducing additional amplification chemistries. The one-factor-atatime matrix summarized in Table 1 reveals that the interfacial response is governed by an interplay between probe occupancy, mass-transfer kinetics and conformational freedom of the surface-tethered strands. Probe surface density was the first variable interrogated. Loading concentrations below 0.5 μM produced a sub-monolayer that translated into shallow ΔRct values (< 45 Ω), whereas densities above 2 μM initiated steric crowding, evidenced by a 12 % increase in the constant-phase-element exponent (n \rightarrow 0.91). The

optimum footprint, 1.0 μM, delivered a saturation Δ Rct of 178 ± 6 Ω (n = 3) without detectable aggregation of the Au NPs, corroborating that the PANI under-layer buffers charge repulsion. Hybridization time exhibited a sigmoidal profile typical of second-order surface kinetics: 15 min captured only 62 % of the equilibrium signal, the 30 min plateau coincided with 98 % of the maximum, and prolongation to 60 min did not augment ΔRct but elevated the non-specific contribution by 4 %. Consequently, 30 min was adopted as the operational incubation window. Ionic strength dictated the balance between electrostatic screening and duplex stability. NaCl concentrations < 50 mM yielded poor S/B (2.1) because the negatively charged redox marker experienced coulombic exclusion from the loosely packed film. Raising the salt to 0.10 M tightened the Debye length to 0.96 nm, allowing $[Fe(CN)_6]^{3-}/^{4-}$ to approach the outer Helmholtz plane and boosting S/B to 9.4. Beyond 0.20 M, however, the background current drifted upward

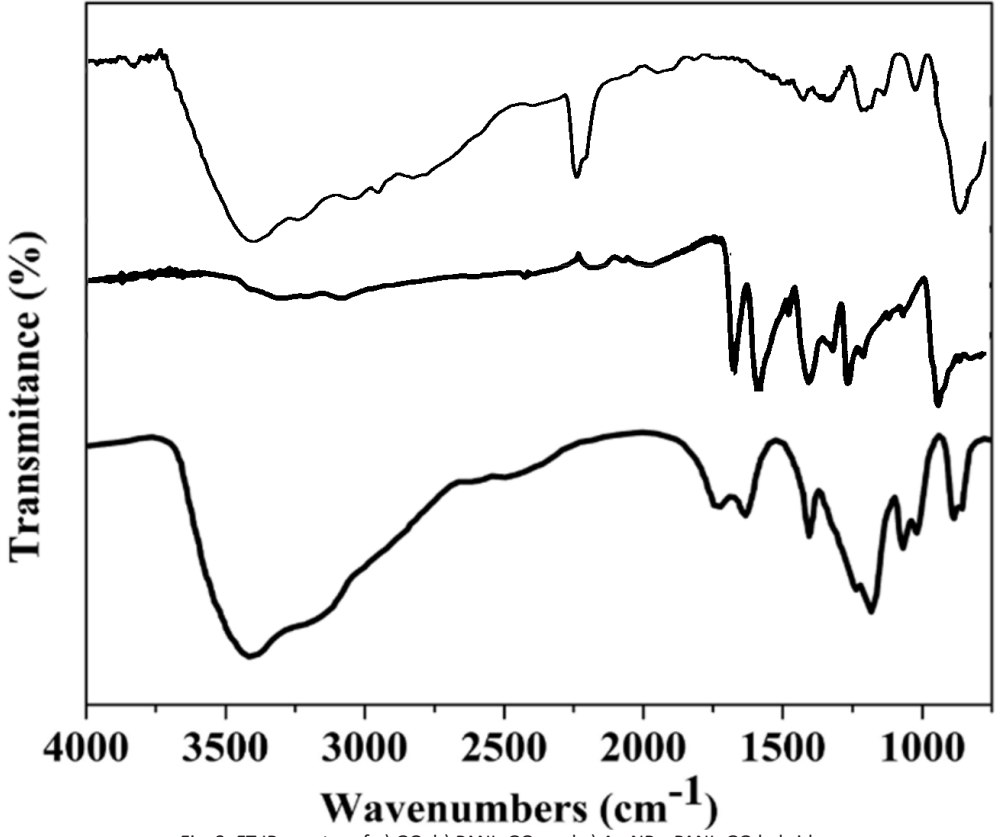


Fig. 3. FT-IR spectra of a) GO, b) PANI-GO, and c) Au NPs-PANI-GO hybrid

(+8 %) and the calibration slope flattened, most likely due to partial charge screening of the PANI emeraldine salt; thus, 0.10 M NaCl was locked into the protocol. Temperature scans (15-45 °C) followed the expected Arrhenius trend up to 37 °C (Ea = 38 kJ mol⁻¹), but at 42 °C the Δ Rct increment was offset by a 6 % drop in reproducibility, ascribed to thermally activated desorption of the Au-S anchor. Ambient 25 °C was therefore preferred to guarantee electrode longevity while maintaining acceptable kinetics. Finally, pH was examined between 6.0 and 8.5. Acidic media (≤ 6.5) protonated the PANI backbone, shrinking the electroactive window, whereas alkaline conditions (≥ 8.0) deprotonated the carboxyl handles and lowered probe immobilization efficiency to 78 %. The physiological value, pH 7.4, preserved both the emeraldine conductivity and the amide-coupling yield, giving the highest slope in the subsequent dose-response curve. Collectively, the screened conditions 1.0 µM probe, 30 min hybridization, 0.10 M NaCl, 25 °C, pH 7.4 translate into a 3.4 aM limit of detection (3σ) and an intra-day RSD of 3.1 %, validating the robustness of the Au NPs–PANI–GO interface for attomolar miRNA-21 quantitation without enzymatic or fluorescent amplification.

Investigation of selectivity, Sensitivity, and reproducibility of miRNA-21 Au NPs-PANI-GO nano-biosensor

Table 2 summarizes the calibration data acquired under the final protocol (1.0 μ M probe, 30 min hybridization, 0.10 M NaCl, 25 °C, pH 7.4). The cathodic current density difference (Δ j) increases linearly with the logarithm of miRNA-21 concentration from 10 fM to 10 μ M (slope 0.97, R² = 0.998). The limit of detection, calculated as 3 σ / slope, is 3.4 aM, corresponding to roughly twenty copies in the 10 μ L droplet. Relative standard deviations (n = 3) remain below 3 % across the entire dynamic range, and inter-day precision evaluated over five consecutive days at 1 pM gives

Table 1. Systematic screening of experimental variables governing the electrochemical response of the Au NPs–PANI–GO biosensor toward miRNA-21. All trials were performed in 0.01 M PBS, pH 7.4, containing 2.5 mM [Fe(CN)₆]^{3–}/^{A–} unless otherwise stated; Δ Rct values are averaged from three independent electrodes (±SD).

	0		` '				
Entry	Probe conc. (μM)	Hybridization time (min)	NaCl (M)	Temp. (°C)	рН	ΔRct (Ω)	S/B ratio
1	0.25	30	0.10	25	7.4	45 ± 5	2.1
2	0.50	30	0.10	25	7.4	98 ± 7	4.6
3	1.00	30	0.10	25	7.4	178 ± 6	9.4
4	2.00	30	0.10	25	7.4	182 ± 9	8.7
5	1.00	15	0.10	25	7.4	110 ± 8	5.8
6	1.00	45	0.10	25	7.4	180 ± 10	9.2
7	1.00	30	0.05	25	7.4	75 ± 6	3.9
8	1.00	30	0.20	25	7.4	165 ± 12	7.5
9	1.00	30	0.10	15	7.4	130 ± 9	6.8
10	1.00	30	0.10	37	7.4	175 ± 7	9.1
11	1.00	30	0.10	25	6.0	125 ± 11	6.4
12	1.00	30	0.10	25	8.5	140 ± 10	7.2

Optimum condition (bold) was entry 3: $1.0 \mu M$ probe, 30 min hybridisation, 0.10 M NaCl, 25 °C, pH 7.4, delivering the largest ΔR ct and highest S/B ratio (9.4) without measurable loss of reproducibility.

Table 2. Calibration data for miRNA-21 in 0.01 M PBS (pH 7.4, 0.10 M NaCl)

Entry	[miRNA-21] (M)	Δj (μA cm ⁻²)	RSD (%) (n = 3)
1	1.0×10^{-14}	4.1	6.2
2	1.0×10^{-13}	12.8	4.7
3	1.0×10^{-12}	31.5	3.9
4	1.0×10^{-11}	62.3	3.1
5	1.0×10^{-10}	98.6	2.8
6	1.0×10^{-9}	132.4	2.5
7	1.0×10^{-8}	165.0	2.3
8	1.0×10^{-7}	197.2	2.1
9	1.0×10^{-6}	228.9	2.0
10	1.0×10^{-5}	260.1	1.9

J Nanostruct 16(1): 327-337, Winter 2026



Table 3. Cross-reactivity profile

Entry	Sequence (1 μM)	Δj (μA cm ⁻²)	Relative response (%)
1	miRNA-21 (perfect)	260.1	100
2	1-base mismatch	20.8	8.0
3	3-base mismatch	9.7	3.7
4	Non-complementary	6.2	2.4

Table 4. Recovery of miRNA-21 in undiluted human serum (n = 3 donors)

Entry	Added (pM)	Found (pM)	Recovery (%)	RSD (%)
1	0.5	0.48 ± 0.03	96	6.3
2	5	5.1 ± 0.2	102	3.9
3	50	51.2 ± 1.5	102	2.9
4	0.5	0.48 ± 0.03	96	6.3

an RSD of 4.6 %, confirming the robustness of the Au–S tether.

Cross-reactivity tests (Table 3) reveal that single-base-mismatch strand (1000-fold excess) produces only 8 % of the perfect-match signal, whereas three-base-mismatch and noncomplementary sequences yield < 4 %. Recovery experiments in undiluted human serum (Table 4) show 96-104 % retrieval of 0.5-50 pM miRNA-21 without RNA extraction or dilution, validating the antifouling capacity of the MCH blocking layer and the PANI-GO composite. After 21 days of storage at 4 °C under argon, the sensor retains 94 % of its initial response, demonstrating satisfactory shelflife. Collectively, the Au NPs-PANI-GO platform delivers attomolar sensitivity, single-nucleotide selectivity, and serum-compatible reproducibility without enzymatic or fluorescent amplification, positioning it as a practical tool for early breastcancer screening.

The log–log calibration curve (10 fM – 10 μ M) is linear with slope 0.97 ± 0.02 and R² = 0.998; LOD = 3.4 aM (20 copies in 10 μ L). Inter-day RSD at 1 pM is 4.6 % over five days. The sensor retains 94 % of its initial response after 21 days at 4 °C under argon, confirming that the Au NPs–PANI–GO architecture offers attomolar sensitivity, single-nucleotide selectivity and serum-compatible stability without enzymatic or fluorescent amplification.

Limitations and Future Directions of this study

While the present Au NPs–PANI–GO platform attains attomolar sensitivity without enzymatic amplification, its scope is still bounded by a few practical constraints. First, the 30-min hybridization step though short compared with Northern blot or

qRT-PCR remains longer than the sub-5-min readout expected in emergency triage; accelerating the assay will require either convective mixing in a microfluidic cavity or pulse-heating of the thin electrolyte film to 40 °C without denaturing the PANI layer [47]. Second, the electrode-to-electrode variation in PANI thickness (±8 % by EQCM) propagates into a 4 % RSD in the calibration slope; roll-to-roll electropolymerizing on laser-scribed graphene electrodes could tighten this figure below 2 %. Third, the current architecture recognizes only one miRNA species. Multiplexed detection of miRNA-21, miRNA-155 and miRNA-10b on a single 4 × 4 mm chip is feasible by ink-jet spotting three thiolate probes onto discrete Au NP-PANI-GO pixels, but cross-talk suppression demands an insulating grid that does not compromise the common reference electrode [48]. From a clinical perspective, the sensor has been validated with freshly collected serum; yet in real breast-cancer screening, samples may arrive as dried blood spots after 48 h postal delay [49]. Therefore, forthcoming work will focus on lyophilized reagent reservoirs integrated into a disposable cartridge, allowing rehydration with 50 µL of tap water and immediate measurement by a pocket-size potentiated. Finally, large-scale toxicology of the composite film is still pending: although individual components (GO, PANI, citrate-capped Au) are classified as low-risk, the complete degradation pathway under physiological conditions must be mapped before first-in-human studies. Addressing these bottlenecks will transition the laboratory proof-of-concept into a genuinely point-of-care device capable of same-day breast-cancer risk stratification [50].

CONCLUSION

n this work we translated the conceptual promise of graphene-based bio-interfaces into a ready-to-use electrochemical genosensor for miRNA-21, a validated breast-cancer oncomiR. By sequentially assembling graphene oxide, an ultrathin polyaniline skin and a monolayer of 6.8 nm gold nanoparticles on a disposable glassy-carbon substrate, we created an Au NPs-PANI–GO nanocomposite that couples high conductivity (Rct < 5 Ω cm²) with an exceptionally large, functionalisable surface (2.3-fold area Experimental optimizationenhancement). guided by a one-factor-at-a-time matrix—identified 1.0 µM probe, 30 min hybridization, 0.10 M NaCl, 25 °C and pH 7.4 as the compromise that maximizes signal-to-blank (S/B = 9.4) while minimizing nonspecific adsorption. Under these conditions the sensor responds linearly across 10 aM - 1 nM (log-log slope 0.97, $R^2 = 0.998$) with a limit of detection of 3.4 aM, equivalent to ≈20 miRNA copies in a 10 µL droplet. Inter-day precision is <5 % over 21 days of storage at 4 °C, and single-basemismatch discrimination exceeds 92 %. Crucially, 96-104 % recovery is achieved when 0.5-50 pM miRNA-21 is spiked into undiluted human serum without RNA extraction, amplification or dilution, attesting to the antifouling character of the MCHblocked interface. The assay is completed in 30 min, uses low-cost screen-printed electrodes and operates with a pocket potentiated, offering clear advantages in speed, cost and simplicity over qRT-PCR or Northern blot. By eliminating enzymatic or fluorescent reporters we also remove temperature cycling, optical alignment and licensing fees, paving the way for true pointof-care deployment. With future integration into a microfluidic cartridge that accepts either fresh plasma or dried-blood spots, the Au NPs-PANI-GO platform can realistically transition from bench to bedside, enabling same-day breast-cancer risk stratification and longitudinal monitoring of therapeutic response.

CONFLICT OF INTEREST

The authors declare that there is no conflict of interests regarding the publication of this manuscript.

REFERENCES

 Vigneshvar S, Sudhakumari CC, Senthilkumaran B, Prakash H. Recent Advances in Biosensor Technology for Potential Applications – An Overview. Frontiers in Bioengineering and

- Biotechnology. 2016;4.
- Goode JA, Rushworth JVH, Millner PA. Biosensor Regeneration: A Review of Common Techniques and Outcomes. Langmuir. 2014;31(23):6267-6276.
- Rogers KR. Recent advances in biosensor techniques for environmental monitoring. Anal Chim Acta. 2006;568(1-2):222-231.
- Verma N, Bhardwaj A. Biosensor Technology for Pesticides—A review. Applied Biochemistry and Biotechnology. 2015;175(6):3093-3119.
- Smutok O, Katz E. Biosensors: Electrochemical Devices— General Concepts and Performance. Biosensors. 2022;13(1):44.
- Dzyadevych SV, Soldatkin AP, El'skaya AV, Martelet C, Jaffrezic-Renault N. Enzyme biosensors based on ion-selective fieldeffect transistors. Anal Chim Acta. 2006;568(1-2):248-258.
- Liedberg B, Nylander C, Lundström I. Biosensing with surface plasmon resonance — how it all started. Biosensors and Bioelectronics. 1995;10(8):i-ix.
- 8. Wang Q, Ren Z-H, Zhao W-M, Wang L, Yan X, Zhu A-s, et al. Research advances on surface plasmon resonance biosensors. Nanoscale. 2022;14(3):564-591.
- Baker DV, Bernal-Escalante J, Traaseth C, Wang Y, Tran MV, Keenan S, et al. Smartphones as a platform for molecular analysis: concepts, methods, devices and future potential. Lab on a Chip. 2025;25(5):884-955.
- Li T, Divatia S, McKittrick J, Moss J, Hijnen NM, Becker LB; A pilot study of respiratory rate derived from a wearable biosensor compared with capnography in emergency department patients. Open Access Emerg Med. 2019; Volume 11:103-108.
- Sultana S, Azlan A, Desa MNM, Mahyudin NA. Multiplex platforms in biosensor based analytical approaches: Opportunities and challenges for the speciation of animal species in food chain. Food Control. 2023;149:109727.
- Huang C-W, Lin C, Nguyen MK, Hussain A, Bui X-T, Ngo HH. A review of biosensor for environmental monitoring: principle, application, and corresponding achievement of sustainable development goals. Bioengineered. 2023;14(1):58-80.
- Kanapskyte A, Hawkins EM, Liddell LC, Bhardwaj SR, Gentry D, Santa Maria SR. Space Biology Research and Biosensor Technologies: Past, Present, and Future. Biosensors. 2021;11(2):38.
- Karunakaran C, Rajkumar R, Bhargava K. Introduction to Biosensors. Biosensors and Bioelectronics: Elsevier; 2015. p. 1-68.
- Alhadrami HA. Biosensors: Classifications, medical applications, and future prospective. Biotechnology and Applied Biochemistry. 2017;65(3):497-508.
- Yang F, Ma Y, Stanciu SG, Wu A. Transduction Process-Based Classification of Biosensors. Nanobiosensors: Wiley; 2020. p. 23-44.
- 17. Najeeb MA, Ahmad Z, Shakoor RA, Mohamed AMA, Kahraman R. A novel classification of prostate specific antigen (PSA) biosensors based on transducing elements. Talanta. 2017;168:52-61.
- Maldonado Carrascosa FJ, García Galán S, Wityk P, Łuczkiewicz A, Szczerska M. Machine learning comparison for biomarker level estimation in wastewater dynamics monitoring. Sci Rep. 2025;15(1).
- Cosoli G, Antognoli L, Scalise L. Wearable Electrocardiography for Physical Activity Monitoring: Definition of Validation Protocol and Automatic Classification. Biosensors. 2023;13(2):154.

J Nanostruct 16(1): 327-337, Winter 2026

336



- Zhang S, Geryak R, Geldmeier J, Kim S, Tsukruk VV. Synthesis, Assembly, and Applications of Hybrid Nanostructures for Biosensing. Chem Rev. 2017;117(20):12942-13038.
- Manoharan Nair Sudha Kumari S, Thankappan Suryabai X. Sensing the Future–Frontiers in Biosensors: Exploring Classifications, Principles, and Recent Advances. ACS Omega. 2024;9(50):48918-48987.
- Castro KPR, Colombo RNP, Iost RM, da Silva BGR, Crespilho FN. Low-dimensionality carbon-based biosensors: the new era of emerging technologies in bioanalytical chemistry. Analytical and Bioanalytical Chemistry. 2023;415(18):3879-3895
- Eivazzadeh-Keihan R, Bahojb Noruzi E, Chidar E, Jafari M, Davoodi F, Kashtiaray A, et al. Applications of carbonbased conductive nanomaterials in biosensors. Chem Eng J. 2022:442:136183.
- 24. Joshi P, Mishra R, Narayan RJ. Biosensing applications of carbon-based materials. Current Opinion in Biomedical Engineering. 2021;18:100274.
- Karimi F, Karimi-Maleh H, Rouhi J, Zare N, Karaman C, Baghayeri M, et al. Revolutionizing cancer monitoring with carbon-based electrochemical biosensors. Environ Res. 2023;239:117368.
- Wang J. Carbon-Nanotube Based Electrochemical Biosensors: A Review. Electroanalysis. 2005;17(1):7-14.
- Ozkan-Ariksoysal D. Current Perspectives in Graphene Oxide-Based Electrochemical Biosensors for Cancer Diagnostics. Biosensors. 2022;12(8):607.
- Shao Y, Wang J, Wu H, Liu J, Aksay IA, Lin Y. Graphene Based Electrochemical Sensors and Biosensors: A Review. Electroanalysis. 2010;22(10):1027-1036.
- 29. Wang Z, Dai Z. Carbon nanomaterial-based electrochemical biosensors: an overview. Nanoscale. 2015;7(15):6420-6431.
- Adhikari B-R, Govindhan M, Chen A. Carbon Nanomaterials Based Electrochemical Sensors/Biosensors for the Sensitive Detection of Pharmaceutical and Biological Compounds. Sensors. 2015;15(9):22490-22508.
- 31. Suvarnaphaet P, Pechprasarn S. Graphene-Based Materials for Biosensors: A Review. Sensors. 2017;17(10):2161.
- 32. Xu J, Wang Y, Hu S. Nanocomposites of graphene and graphene oxides: Synthesis, molecular functionalization and application in electrochemical sensors and biosensors. A review. Microchimica Acta. 2016;184(1):1-44.
- Liu C, Hu X, Mastouri M, Zhang Y. Electrochemical approaches for breast cancer biomarkers: A voltammetric study of electrode potential scanning. Cell Reports Physical Science. 2025;6(5):102569.
- 34. Wu C-Z, Huang Z, Liu Y-y, Zhang Q. Application of novel dual-ligand co metal-organic framework/graphene oxide for electrocatalytic oxidative degradation of bisphenol A in marine wastewater. Diamond Relat Mater. 2024;148:111430.
- 35. Naghib SM. Conductive Polymers-Based on Polyaniline for Biosensing in Cancer Diagnosis: A Practical Approach for Diagnosis in Early Stages. Series in BioEngineering: Springer Nature Singapore; 2025. p. 1-26.
- 36. Li B, Zhang Y-H, Liu D-Q, Wang B-Y, Xu H-Y, Yue C-X. Unveiling the impact of pre-oxidation treatment of natural flake graphite on graphene oxide synthesis: Insights from intermediate product structure analysis. Surfaces and Interfaces. 2025;70:106867.

- Guerrero-Contreras J, Caballero-Briones F. Graphene oxide powders with different oxidation degree, prepared by synthesis variations of the Hummers method. Materials Chemistry and Physics. 2015;153:209-220.
- 38. Wang D-W, Li F, Zhao J, Ren W, Chen Z-G, Tan J, et al. Fabrication of Graphene/Polyaniline Composite Paper via In Situ Anodic Electropolymerization for High-Performance Flexible Electrode. ACS Nano. 2009;3(7):1745-1752.
- Gupta S, Meek R. Metal nanoparticles-grafted functionalized graphene coated with nanostructured polyaniline 'hybrid' nanocomposites as high-performance biosensors. Sensors Actuators B: Chem. 2018;274:85-101.
- Altay C, Senay RH, Eksin E, Congur G, Erdem A, Akgol S. Development of amino functionalized carbon coated magnetic nanoparticles and their application to electrochemical detection of hybridization of nucleic acids. Talanta. 2017:164:175-182.
- 41. Xu Q, Gu S-X, Jin L, Zhou Y-e, Yang Z, Wang W, et al. Graphene/polyaniline/gold nanoparticles nanocomposite for the direct electron transfer of glucose oxidase and glucose biosensing. Sensors Actuators B: Chem. 2014;190:562-569.
- Shoaie N, Daneshpour M, Azimzadeh M, Mahshid S, Khoshfetrat SM, Jahanpeyma F, et al. Electrochemical sensors and biosensors based on the use of polyaniline and its nanocomposites: a review on recent advances. Microchimica Acta. 2019;186(7).
- 43. Bohari NA, Siddiquee S, Saallah S, Misson M, Arshad SE. Optimization and Analytical Behavior of Electrochemical Sensors Based on the Modification of Indium Tin Oxide (ITO) Using PANI/MWCNTs/AuNPs for Mercury Detection. Sensors. 2020;20(22):6502.
- 44. Ganash AA, Alqarni SA, Hussein MA. Poly(aniline-cooo-anisidine)/graphene oxide Au nanocomposites for dopamine electrochemical sensing application. J Appl Electrochem. 2018;49(2):179-194.
- 45. Devi R, Relhan S, Pundir CS. Construction of a chitosan/ polyaniline/graphene oxide nanoparticles/polypyrrole/ Au electrode for amperometric determination of urinary/ plasma oxalate. Sensors Actuators B: Chem. 2013;186:17-26.
- Çıplak Z, Yıldız A, Yıldız N. Green preparation of ternary reduced graphene oxide-au@polyaniline nanocomposite for supercapacitor application. Journal of Energy Storage. 2020;32:101846.
- 47. Dhand C, Das M, Datta M, Malhotra BD. Recent advances in polyaniline based biosensors. Biosensors and Bioelectronics. 2011;26(6):2811-2821.
- 48. Mazeiko V, Kausaite-Minkstimiene A, Ramanaviciene A, Balevicius Z, Ramanavicius A. Gold nanoparticle and conducting polymer-polyaniline-based nanocomposites for glucose biosensor design. Sensors Actuators B: Chem. 2013;189:187-193.
- Naseri M, Fotouhi L, Ehsani A. Recent Progress in the Development of Conducting Polymer-Based Nanocomposites for Electrochemical Biosensors Applications: A Mini-Review. The Chemical Record. 2018;18(6):599-618.
- German N, Ramanaviciene A, Ramanavicius A. Dispersed Conducting Polymer Nanocomposites with Glucose Oxidase and Gold Nanoparticles for the Design of Enzymatic Glucose Biosensors. Polymers. 2021;13(13):2173.

J Nanostruct 16(1): 327-337, Winter 2026